Proceedings of the Seventh International Conference on
Railway Technology: Research, Development and Maintenance
Edited by: J. Pombo
Civil-Comp Conferences, Volume 15, Paper 3.12
Civil-Comp Press, Edinburgh, United Kingdom, 2026
ISSN: 2753-3239, doi: 10.4203/ccc.15.3.12

Study on Fatigue Crack Growth Behavior in Rails Using a Fracture Phase-Field Method

J. Yang, J. Xu and P. Wang

**Southwest Jiaotong University,
Chengdu, People's Republic of China**

Abstract

This paper shows the development of a numerical model for fatigue crack growth in rails under rolling contact loading based on the fracture phase-field method, which accounts for fatigue damage accumulation. Within a thermodynamically consistent phase-field framework, a fatigue degradation function is introduced to describe the attenuation of material fracture energy under cyclic loading. The implicit solution of the damage field under moving Hertzian contact loads is implemented through ABAQUS user subroutines, combined with a cycle-jumping algorithm. Numerical results indicate that cracks initiate in the subsurface region at a depth of approximately 0.65 times the contact half-width, subsequently branch into disordered crack networks, and eventually exhibit a bidirectional propagation pattern extending both downward toward the rail foot and upward toward the running surface, which aligns well with the characteristics of squat-type damage in rails. The model effectively reveals the transformation mechanism from subsurface cracking to surface spalling, offering a numerical tool for understanding rolling contact fatigue damage mechanisms in rails, although it does not yet consider actual non-Hertzian contact profiles or surface material hardening. Despite these simplifications, this study successfully elucidates the evolution of subsurface-to-surface crack propagation.

Keywords: rail, fracture phase-field, rolling contact fatigue, subsurface crack initiation and propagation, numerical simulation, cycle-jumping algorithm

1 Introduction

Railway rails are a core component of the railway transportation system and play a crucial role. They serve not only as the track foundation for train operation, providing stable guidance to ensure that trains run smoothly along predetermined routes and avoid derailment, but also as critical infrastructure bearing train loads [1]. Under long-term service conditions, rails are subjected to cyclic wheel loads, making the rail surface prone to fatigue cracks [2]. In severe cases, these cracks can compromise operational safety. Therefore, accurately predicting the development of rail fatigue cracks is of great significance for the safe operation of railway trains.

In recent years, the fracture phase-field method [3] has gained increasing attention in fracture mechanics due to its advantages in simulating crack initiation and complex crack paths. Originating from the variational fracture theory based on energy minimization, this method introduces a scalar phase-field variable into the continuum, transforming the originally discrete crack surface with unknown topology into a diffused damage band of finite width. This avoids explicit crack tracking and mesh reconstruction, enabling natural modeling of crack initiation, propagation, branching, and coalescence.

Building on this, scholars such as Lo [4], Schreiber [5], and Khalil [6] introduced fatigue damage accumulation mechanisms into the phase-field framework, proposing a series of phase-field models for describing metal fatigue crack growth. These models can reproduce Paris' law, S–N curves, and fatigue responses under multi-level loading. Cui et al. [7] systematically reviewed recent advances in the fatigue phase-field method, highlighting its broad applicability in structural macro-, material micro-, and multi-scale fatigue problems. Some researchers further developed phase-field models for high-cycle and very-high-cycle fatigue, integrating local stress–strain methods, fatigue damage accumulation theory, and classical S–N/ε–N data into the degradation process of fracture energy. Combined with numerical strategies such as envelope loading and cycle jumping, these models enable the simultaneous prediction of fatigue life and Paris-type crack growth behavior in the high-cycle fatigue regime, thereby significantly advancing the application and promotion of the phase-field method in engineering fatigue problems [8].

Compared with the relatively mature applications mentioned above, research directly applying the fracture phase-field method to the study of rolling contact fatigue crack growth in railway rails remains limited. Only a few studies have simulated pitting and spalling behaviors in components such as gears based on the phase-field framework [9-11]. For rail structures with complex railhead geometries and actual wheel–rail moving contact loads, research is still scarce. In light of this, this paper establishes a rail rolling contact fatigue crack model considering actual wheel–rail contact loads based on the fracture phase-field method. Through numerical simulations, the crack initiation and propagation behavior are investigated, and the influence of key service parameters on fatigue life and crack morphology evolution is revealed. This work provides theoretical foundations and methodological support for the analysis of rail fatigue damage mechanisms and life prediction.

2 Methods

The phase-field method is based on the principle of energy minimization, where a continuous scalar field variable is introduced to diffusely describe the crack topology, thereby avoiding the numerical difficulties associated with traditional fracture mechanics in handling complex crack paths. This section builds a fracture mechanics model suitable for elastoplastic rail materials based on the variational fracture theory proposed by Francfort and Marigo [12] , combined with the phase-field model framework with energy threshold proposed by Miehe et al. [13]. To describe the crack topology within the continuum, a scalar phase-field variable $\phi(x,t) \in [0,1]$ is introduced. Here, $\phi = 0$ represents intact material, and $\phi = 1$ indicates a fully fractured state. To overcome the limitation of standard phase-field models where damage occurs even during the elastic stage, this study adopts a phase-field model with a stress threshold, as illustrated in Figure 1.

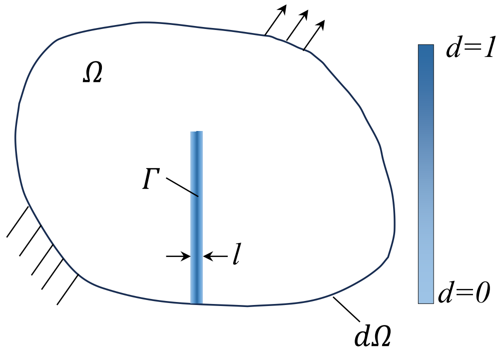

Figure 1: Schematic illustration of a solid body with a diffused crack

For an elastoplastic solid, the total potential energy functional Π is composed of the stored elastoplastic energy Π^b and the dissipated energy Π^f:

$$\Pi(\boldsymbol{u},\phi) = \int_{\Omega} [g(\phi)\psi^+ + \psi^-]\, d\Omega + \int_{\Omega} \psi_c [2\phi + l^2|\nabla\phi|^2]\, d\Omega \tag{1}$$

Here, $g(\phi)$ is the stiffness degradation function, taken in quadratic form as $g(\phi) = (1-\phi)^2 + k$, where k is a residual stiffness coefficient introduced to avoid numerical singularity (set to 0.01 in this study). ψ^+ denotes the effective elastoplastic strain energy density driving crack propagation, while ψ^- represents the residual strain energy density that does not participate in stiffness degradation. The parameter l is the phase-field length scale controlling the width of the diffused crack band; it is generally taken as three times the element size and is set to 0.3 mm here. ψ_c is the critical fracture energy density per unit volume, related to the material's critical energy release rate G_c by:

$$\psi_c = \frac{3G_c}{8\sqrt{2}l} \tag{2}$$

Under the small-strain assumption, the strain tensor is decomposed as $\varepsilon = \varepsilon^e + \varepsilon^p$. The plastic behavior of the rail steel is described using the J_2 flow rule and an isotropic hardening criterion. The yield function is defined as:

$$F = \bar{\sigma}_{eq} - \sigma_y(\bar{\varepsilon}^p) \leq 0 \tag{3}$$

where $\bar{\sigma}_{eq}$ is the effective von Mises equivalent stress, $\sigma_y(\bar{\varepsilon}^p)$ is the current yield stress evolving with the equivalent plastic strain $\bar{\varepsilon}^p$, and $\bar{\varepsilon}^p$ is the accumulated equivalent plastic strain.

The wheel–rail contact region experiences high hydrostatic pressure. To prevent non-physical “self-healing” of crack surfaces under compression, the model must strictly distinguish between volumetric and deviatoric deformations. This study adopts a volumetric–deviatoric decomposition scheme

The driving energy ψ^+ is defined as the sum of the elastic deviatoric strain energy and the plastic dissipation work:

$$\psi^+(\varepsilon, \bar{\varepsilon}^p) = \mu(\varepsilon_{dev}^e : \varepsilon_{dev}^e) + \psi_p(\bar{\varepsilon}^p) \tag{4}$$

The residual energy ψ^- is defined as the elastic volumetric strain energy (regardless of tension or compression):

$$\psi^-(\varepsilon) = \frac{1}{2} K[tr(\varepsilon^e)]^2 \tag{5}$$

Based on this energy decomposition, the update rule for the Cauchy stress tensor σ involves degradation only of the deviatoric stress component:

$$\sigma = g(\phi)s^e + p^e I \tag{6}$$

where $\mathbf{s}^e = 2\mu\varepsilon_{\mathrm{dev}}^e$ is the effective elastic deviatoric stress tensor, and $p^e = K\,\mathrm{tr}(\varepsilon^e)$ is the effective hydrostatic pressure.

Taking the variation $\delta\phi$ of the total potential energy functional Π with respect to ϕ and applying the Euler–Lagrange equation, the strong form governing the evolution of the phase field can be derived.

The variational condition $\delta\Pi = 0$ yields:

$$-(1-\phi)\frac{\psi^+}{\psi_c} + 1 - l^2\nabla^2\phi = 0 \tag{7}$$

Rearranging gives a Helmholtz-type partial differential equation:

$$-l^2\nabla^2\phi + [1 + \mathcal{H}]\phi = \mathcal{H} \tag{8}$$

Here, the dimensionless crack driving force state function $\mathcal{H}$, i.e., the history field, is defined as:

$$\mathcal{H} = \max_{\tau\in[0,t]} \left\langle \frac{\psi^+}{\psi_c} - 1 \right\rangle \tag{9}$$

In the above, $\langle\cdot\rangle$ denotes the Macaulay bracket. Damage ϕ initiates only when the driving energy density ψ^+ exceeds the threshold ψ_c, making $\mathcal{H} > 0$.

To simulate fatigue crack initiation under cyclic loading, this study introduces an energy-dissipation-based fatigue accumulation theory into the phase-field framework.

The model assumes that the material's fracture resistance gradually degrades with fatigue cycles. This is achieved by modifying the critical fracture energy G_c (i.e., the threshold ψ_c) via a fatigue degradation function $\alpha(D)$:

$$\psi_c(D) = \frac{3G_c \cdot \alpha(D)}{8\sqrt{2}l} \tag{10}$$

The degradation function $\alpha(D)$ follows a power-law form:

$$\alpha(D) = (1-\alpha_0)(1-D)^{\xi} + \alpha_0 \tag{11}$$

where $D \in [0,1]$ is a local fatigue accumulation variable, α_0 is the residual toughness coefficient after fatigue failure (taken as 0.001 here), and ξ is a shape parameter. As D increases, ψ_c decreases, allowing regions originally in the elastic state ($\psi^+ < \psi_c^{\text{initial}}$) to gradually satisfy the failure criterion $\psi^+ > \psi_c(D)$, thereby simulating the natural initiation of fatigue cracks.

The evolution of the local fatigue variable D follows Miner's linear cumulative rule. The damage increment per cycle ΔD is determined by the Basquin equation:

$$\Delta D = \frac{1}{N_f}, \quad N_f = \left(\frac{\sigma_f'}{\sigma_{eq}}\right)^{1/a} \tag{12}$$

In this study, the fatigue strength coefficient σ_f' is set to 907MPa, and the fatigue strength exponent a is 0.901.

3 Methods

To simulate fatigue crack initiation and propagation in rails under cyclic wheel–rail contact loading, a two-dimensional plane-strain finite element model was established within the ABAQUS/Standard implicit analysis framework.

The model employs a two-layer shared-node scheme to couple the displacement field and the phase field. The displacement field is discretized using 4-node plane-strain elements (CPE4), and the elastoplastic constitutive behavior, stress update, and plastic dissipation are described via a user material subroutine (UMAT). The phase field is approximated by user-defined elements overlapped at the same nodal positions, with its evolution equation solved through a user element subroutine (UEL). A history field variable is introduced to ensure the irreversibility of damage.

To balance computational accuracy and efficiency, a locally refined mesh strategy is adopted. In the refined zone (contact region and potential crack growth area) – i.e., the rail surface and subsurface – the element size is set to 0.1 mm. This dimension is smaller than the phase-field length scale parameter, sufficient to capture the gradient of the diffused crack band and to accurately resolve local contact stress gradients. In the transition and far-field regions, the mesh size is gradually increased to reduce the total number of degrees of freedom. The bottom boundary of the model is fully constrained ($U_x = U_y = 0$), while symmetric boundary conditions ($U_x = 0$) are applied on the left and right sides to simulate the restraint effect of a continuous rail, as illustrated in Figure 2.

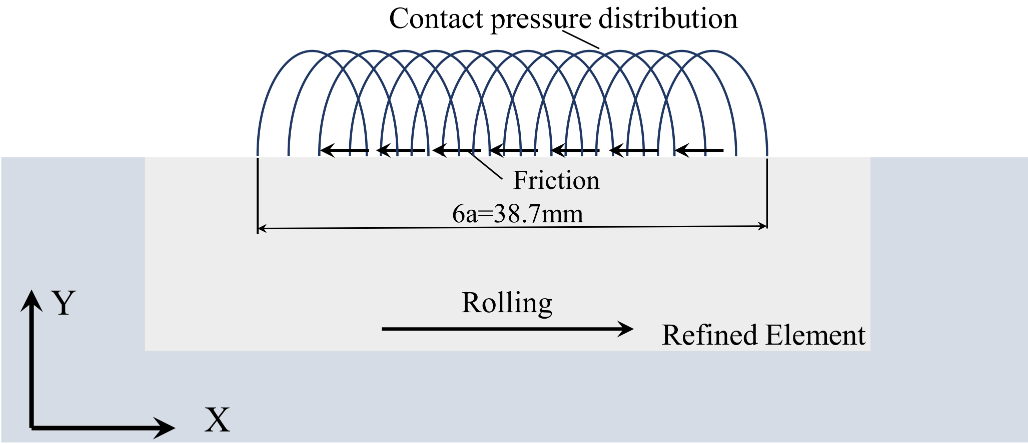

Figure 2: Schematic of wheel–rail rolling contact loading

The wheel–rail contact is simplified as a cylinder-on-plane configuration. Instead of modeling the wheel as a solid body, moving surface tractions are directly applied on the rail top surface through user-defined distributed load subroutines **DLOAD** and **U TRACLOAD**.

The normal contact pressure $p(x)$ follows the Hertzian distribution:

$$p(x) = p_0 \sqrt{1 - \left(\frac{x - x_c}{a}\right)^2}, \quad |x - x_c| \leq a \tag{13}$$

where p_0 is the maximum contact pressure (set to **800 MPa** in this study), a is the Hertzian contact half-width (taken as **6.25 mm**), and x_c denotes the current load-center position.

The tangential traction $q(x)$ is applied according to Coulomb's friction law:

$$q(x) = \mu \cdot p(x) \tag{14}$$

with a friction coefficient $\mu = 0.1$, acting in the rolling direction to simulate traction conditions.

To realistically simulate the entire wheel-passing process, the load center x_c moves c ontinuously within each analysis step (Step) along the increment sequence (Incremen t). The moving range extends from –2a to +2a relative to the contact center. This inte rval (four times the contact half-width) ensures that material points of interest underg o a complete "loading–unloading–residual-stress-building" cycle. Pseudo-time step c ontrol is implemented: a single pass is discretized into N_{steps} increments (e.g., 50 step s in the code). The load position is periodically reset using the modulo function (MO D) to enable multi-pass continuous loading simulation:

$$x_c(k) = x_{start} + \frac{x_{end} - x_{start}}{N_{steps}} \cdot \text{mod}\left(k - 1, N_{steps}\right) \tag{15}$$

This approach avoids abrupt stress-field changes caused by traditional discrete loading steps and ensures a smooth evolution of the crack driving force.

Since high-cycle fatigue (HCF) involves millions of cycles, cycle-by-cycle computation is computationally prohibitive. An adaptive cycle-jumping algorithm is implemented in the UMAT and UEL subroutines to dynamically adjust the computational step size ΔN according to the accumulation rate of the phase-field damage.

In each load increment, the fatigue damage increment per cycle, $\mathrm{d}D/\mathrm{d}N$, is first evaluated based on the current stress state using the Basquin equation. The damage is then extrapolated over the jump step ΔN:

$$D_{n+1} = D_n + \Delta N \cdot \frac{\mathrm{d}D}{\mathrm{d}N} \tag{16}$$

The accumulated fatigue variable D reduces the material's fracture toughness G_c through the degradation function $\alpha(D)$, thereby lowering the critical energy threshold ψ_c for phase-field evolution.

To address the strong nonlinear convergence issues in the later stages of crack initiation, the algorithm divides the computation into three phases based on the current global maximum phase-field value $\phi_{\max}$:

Phase 1 ($\phi_{\max} < 0.1$): The material is in the early stage of fatigue damage accumulation without macroscopic cracking. A relatively large baseline step size ($\Delta N = 100000$) is used to rapidly consume fatigue life.

Phase 2 ($0.1 \le \phi_{\max} \le 0.9$): Cracks have initiated and begun to propagate stably. To accurately capture the crack path and prevent numerical oscillations, the jump step is forcibly reduced (e.g., $\Delta N = 100$).

Phase 3 ($\phi_{\max} > 0.9$): The material approaches complete fracture with sharply degraded stiffness. The step size is reduced to a very small value ($\Delta N = 1$), or even reverts to cycle-by-cycle computation, to ensure convergence of the Newton-Raphson iteration and to accurately capture the final fracture.

4 Results

The numerical simulation based on the fracture phase-field method successfully reproduces the entire process of fatigue damage in rails under moving wheel–rail contact loading. Fig. 3(a)–(d) presents the evolution characteristics of rail cracks from initiation to propagation under rolling contact loading.

As shown in Fig. 3(a), the crack first initiates in the subsurface region at a depth of approximately 4.3 mm, which corresponds to about 0.65 times the contact half-width. This indicates that the initial damage is controlled by the subsurface high-shear-stress/mixed-stress concentration zone. It should be noted that this study does not explicitly consider surface evolution mechanisms such as plastic shakedown and surface hardening. Therefore, the inhibitory effect of surface strengthening and residual compressive stress on surface crack initiation is not captured, making subsurface initiation more pronounced in the simulation.

As rolling cycles proceed, the crack extends from the initiation zone and exhibits significant branching. Fig. 3(b) shows the first branching of the crack, accompanied by clear longitudinal propagation along the rolling direction, along with an increase in transverse expansion. Fig. 3(c) further displays secondary branching, forming a multi-branch crack network with irregular and non-directional propagation paths. This behavior is attributed to the non-proportional cyclic loading induced by moving contact and the mixed-mode driving under frictional shear, leading to continuous redistribution of stress and energy release rate near the crack tip, which promotes crack deflection and branching.

Finally, as illustrated in Fig. 3(d), after multi-branch evolution, the crack exhibits bidirectional propagation—extending both deeper into the rail head and upward toward the running surface. On one hand, it continues to propagate into the rail interior; on the other hand, it turns upward and tends to connect with the running surface, forming a potential surface failure channel.

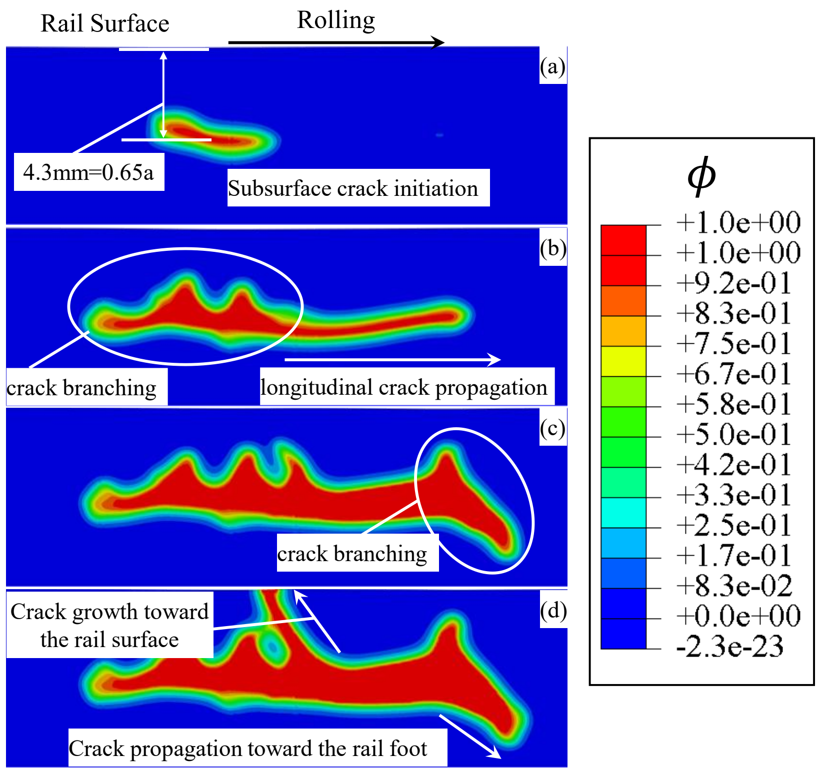

Figure 3: Phase field simulation of fatigue crack initiation and propagation evolution under wheel-rail rolling contact.

5 Conclusions and Contributions

The described process of "subsurface initiation – longitudinally dominated propagation – multiple branching – bidirectional evolution toward the surface and interior" corresponds well with the typical characteristics of squat-type damage in rails. That is, local "depressions/dark spots" may appear on the running surface, accompanied by a complex subsurface crack network, which may further extend into the rail head or penetrate to the surface, leading to failure modes such as spalling or material drop-out.

Based on a thermodynamically consistent fracture phase-field theory, this study numerically reproduces the entire evolution process of rolling contact fatigue (RCF) cracks in rails. The simulation results confirm that, without considering surface gradient hardening, fatigue cracks preferentially initiate in the subsurface region dominated by shear stress, at a depth of approximately 4.3 mm (i.e., 0.65 a) below the running surface. With increasing load cycles, the cracks undergo unstable branching and disordered network-like propagation driven by compressive-shear stress fields, eventually exhibiting a "bidirectional competitive" evolution pattern—extending both deeper into the rail foot and upward toward the running surface. This finding visually reveals the "inside-out" formation mechanism of material spalling and local collapse in squat-type damage, confirming that subsurface crack networks are a key contributing factor to such defects.

At the methodological level, this work establishes a fatigue–fracture coupled phase-field numerical framework suitable for moving load conditions. By implementing an adaptive cycle-jumping algorithm in ABAQUS user subroutines, the time-scale bottleneck in high-cycle fatigue simulation is effectively overcome, enabling continuous modeling of RCF from microscopic damage accumulation to macroscopic topological evolution. The proposed model addresses the numerical difficulties faced by traditional fracture mechanics in handling complex crack topologies such as branching and coalescence, providing an effective theoretical tool for understanding disordered crack propagation under complex stress states and for predicting fatigue life.

Although the study successfully captures the core evolution patterns of cracks, certain limitations remain due to modeling assumptions. The current simulation employs a simplified Hertzian contact model and does not yet account for surface shakedown and work-hardening effects induced by long-term operation, which differ from the actual complex non-Hertzian contact profiles and material gradient properties in real track conditions. Future work will focus on incorporating realistic wheel–rail wear profiles and gradient plastic constitutive models, as well as exploring multi-physics coupling mechanisms, to further enhance the predictive accuracy and applicability of the model in complex engineering environments.

Acknowledgements

The authors acknowledge the financial support provided by the National Natural Science Foundation of China (U2568212, 52388102, 52478474, 52472458).

References

[1] J. Xu, Q. Ma, X. Wang, J. Chen, R. Chen, P. Wang, X. Wei, Investigation on the motion conditions and dynamic interaction of vehicle and turnout due to

differential wheelset misalignment, Vehicle System Dynamics 60(8) (2022) 2587-2607.
[2] X. Deng, Z. Li, Z. Qian, W. Zhai, Q. Xiao, R. Dollevoet, Pre-cracking development of weld-induced squats due to plastic deformation: Five-year field monitoring and numerical analysis, International Journal of Fatigue 127 (2019) 431-444.
[3] B. Bourdin, G.A. Francfort, J.J. Marigo, Numerical experiments in revisited brittle fracture, Journal of the Mechanics and Physics of Solids 48(4) (2000) 797-826.
[4] Y.-S. Lo, M.J. Borden, K. Ravi-Chandar, C.M. Landis, A phase-field model for fatigue crack growth, Journal of the Mechanics and Physics of Solids 132 (2019) 103684.
[5] C. Schreiber, C. Kuhn, R. Müller, T. Zohdi, A phase field modeling approach of cyclic fatigue crack growth, International Journal of Fracture 225(1) (2020) 89-100.
[6] Z. Khalil, A.Y. Elghazouli, E. Martínez-Pañeda, A generalised phase field model for fatigue crack growth in elastic–plastic solids with an efficient monolithic solver, Computer Methods in Applied Mechanics and Engineering 388 (2022) 114286.
[7] H. Cui, C. Du, H. Zhang, Applications of Phase Field Methods in Modeling Fatigue Fracture and Performance Improvement Strategies: A Review, Metals, 2023, p. 714.
[8] W. Tang, M. Yi, L.-Q. Chen, W. Guo, Classical fatigue theory informed phase-field model for high-cycle fatigue life and fatigue crack growth, Engineering Fracture Mechanics 306 (2024) 110212.
[9] Z. Zhang, G.-Y. Huang, F. Shen, L.-L. Ke, A phase field model for spalling failure due to rolling contact fatigue, International Journal of Fatigue 198 (2025) 109006.
[10] T. Polančec, T. Lesičar, Z. Tonković, S. Glodež, Modelling of rolling-contact fatigue pitting phenomena by phase field method, Wear 532-533 (2023) 205068.
[11] T. Schneider, D. Müller, M. Seiler, T. Tobie, K. Stahl, M. Kästner, Phase-field modeling of fatigue crack growth during tooth flank fracture in case-hardened spur gears, International Journal of Fatigue 163 (2022) 107091.
[12] G.A. Francfort, J.J. Marigo, Revisiting brittle fracture as an energy minimization problem, Journal of the Mechanics and Physics of Solids 46(8) (1998) 1319-1342.
[13] C. Miehe, L.-M. Schänzel, H. Ulmer, Phase field modeling of fracture in multi-physics problems. Part I. Balance of crack surface and failure criteria for brittle crack propagation in thermo-elastic solids, Computer Methods in Applied Mechanics and Engineering 294 (2015) 449-485.